A Study on the Radiation Effect of the Smoke Movement in Room Fires

Jin Yong Jeong* and Hong Sun Ryou*

Key words: SMEP, PISO algorithm, Discrete ordinate method, Radiation effect

Abstract

To investigate smoke movement with radiation in a room fires, a numerical and experimental analysis were performed. In this paper, results from a field model based on a self-developed SMEP (Smoke Movement Estimating Program) were compared with Steckler's experiment and the experiments on various sized pool fires in a room with door. The SMEP using PISO algorithm solves conservation equations for mass, momentum, energy and species, together with those for the modified $k-\varepsilon$ turbulence model with buoyancy term. Also it solves the radiation equation using the S-N discrete ordinates method (DOM). The result of the calculated smoke temperature considering radiation effect has shown good agreement compared with the experimental data, although there are large discrepancy in the hot smoke layer between the temperature predicted by the SMEP with only convection effect and obtained by the experimental result. This large discrepancy is caused from the radiation effect of H_2O and CO_2 gas under smoke productions. Hence the radiation effect under smoke in fire is the point to be specially considered in order to produce more realistic result.

Nomenclature

A : fire source area [m^2]
$a_{\varepsilon,i}$: emissivity weighting factors for the i-th gray gas
C_P : specific heat of plume gases [kJ/kgK]
D_f : diameter of fire [m]
I_w : wall radiation intensities [W/(m^2 · sr)]
$\dot{m}$: mass flow rate [kg/s]
Q : heat release rate of the fire [kW]
Q_c : convective of the heat release rate [kW]
T_w : wall temperature [K]
T_{Zf} : average plume temperature at elevation, Z_{fl} [K]
T_∞ : ambient temperature [K]
t : time [sec]
v : vertical upward speed at height, Z_{fl} [m/s]
Z_{fl} : mean flame height [m]

Greek symbols

ε_w : wall emissivity
κ_i : absorption coefficient for the i-th gray gas

* Department of Mechanical Engineering, Chung-Ang University, 221 Huksuk-Dong, Dongjak-Ku, Seoul 156-756, Korea

ρ_∞ : density of ambient gas [kg/m^3]
$\triangle \tau_i$: cell volume [m^3]
Ω, Ω' : scattering and incoming/outgoing direction

1. Introduction

The control of smoke movement in a room fires is often an important factor of designing efficient fire protection systems. The prevention of fires in rooms requires an understanding and prediction of the temperature field and smoke concentration by the fire and the air flow through openings. Recent studies of fire plumes by Zukoski et al.[1] and Quintiere et al.[2] have shown that buoyant diffusion flames tend to entrain air more than an idealized point source plume, and that the smoke flow is influenced by fire strength and laboratory atmospheric disturbances. Yang,[3] Kerrison et al.[4] and Ewer et al.,[5] studied several field models including PHOENICS, FLOW3D, SMARTFIRE and UNDSAFE and discussed the limitations and capabilities of the fire models. However, their studies have neglected a radiative heat transfer mechanisms and focused on the comparison and evaluation of overall ability of the commercial CFD program. Consequently, what seems to be lacking in fire modeling is an effect of radiative heat transfer and suitable experimental benchmark fire data. In field modeling, sub-models of combustion, turbulence and radiative heat transfer are needed to describe a fire phenomenon. One of the reasons why an enclosure fire is a complex phenomenon is that there are strong interactions among these three effects. Xue et al.[6] studied the comparison of various combustion models in enclosure fire simulation. The difficulty of turbulent combustion model is due to the nature of enclosure fire phenomena where pyrolysis and gasification are inherent and very complex to model. Furthermore it is not easy to accurately know the reaction kinetics and combustion rate in a room fires. In the present study, physically controlled diffusion flame model[7,8] including combustion based on the global single-step irreversible reaction was applied. Turbulence model used the modified $k-\varepsilon$ turbulence model with buoyancy term.

Radiation is an important heat transfer mode to represent in fire modeling due to the high temperatures attained in rooms with fires or hot smoke layers. Predicting possible secondary ignition due to thermal radiation is particularly important in fire safety engineering, because it enables protection of adjacent material from igniting. Lockwood et al.,[9] Hoffmann et al.,[10] Forney[11] and Keramida et al.[12] investigated a radiative heat transfer occurring in a fire modeling and conducted intensive comparison and evaluation with fire experimental data. Isotropic scattering cases of radiative transfer in two-dimensional rectangular room were studied by Fiveland,[13] using the S-N discrete ordinates method and Thynell and Ozisik,[14] by using the finite element method. Three-dimensional P-3 results were reported by Menguc and Viskanta.[15] For radiation model in this study, the S-N discrete ordinate method based on the weighed sum of gray gas model (WSGGM)[16] used.

The aim of the present study is to examine the effect of radiative heat transfer on smoke movement in three dimensional room fires. Results from a self-developed SMEP (Smoke Movement Estimating Program) field model using DOM radiation model and PISO algorithm were compared with data obtained from the room fire experiments of Steckler[17] and the various sized pool fire experiments using methanol as a fuel in a room with door.

2. The experiments

The room dimensions were 1.8 m×1.8 m in plan and 1.38 m in height with the 1.18 m high by 0.48 m wide door. The wall was made of

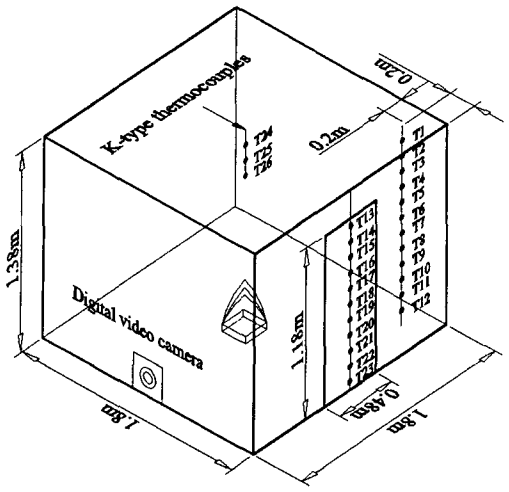

Fig. 1 Experimental arrangements and configurations.

about 10 mm thick acryl and asbestos slates. Three experiments were conducted in which the fire size was varied (7.65, 21.25, 51.71 kW). Figure 1 shows the overall arrangement of measurement probes and room geometry. The fuel tray were made of 2 mm thick steel plate and placed in the center of floor. Sizes of tray, 15 ×15 cm, 25×25 cm, 39×39 cm surface area and 7 cm deep were used to vary the fuel surface area. Methanol (purity 99.9%) was used as the fuel. The mass burning rate of fuel was evaluated by measuring the weight of the fuel vessel continuously using the load cell. K-type thermocouples (measurement limits: −270~1300 ℃) with a wire diameter of 0.32 mm were placed in the center line vertically of the door and in the front corner of the room to measure the gas temperature profile.

3. The mathematical models

3.1 Flow field model

The flow is described by the three-dimensional, Favre-averaged equations of transport

Table 1 The flux and source terms for the conservation equations

Φ	Γ_Φ	S_Φ
1	0	0
u	μ_{eff}	$-\frac{\partial p}{\partial x}+\frac{\partial}{\partial x}\left(\mu_{eff}\frac{\partial u}{\partial x}\right)+\frac{\partial}{\partial y}\left(\mu_{eff}\frac{\partial v}{\partial x}\right)+\frac{\partial}{\partial x}\left[\mu_{eff}\frac{\partial u}{\partial x}-\frac{2}{3}(\rho k+\mu_{eff}\nabla\cdot\vec{u})\right]$
v	μ_{eff}	$-\frac{\partial p}{\partial y}+\frac{\partial}{\partial x}\left(\mu_{eff}\frac{\partial u}{\partial y}\right)+\frac{\partial}{\partial y}\left(\mu_{eff}\frac{\partial w}{\partial y}\right)+\frac{\partial}{\partial y}\left[\mu_{eff}\frac{\partial v}{\partial y}-\frac{2}{3}(\rho k+\mu_{eff}\nabla\cdot\vec{u})\right]$
w	μ_{eff}	$-\frac{\partial p}{\partial z}+\frac{\partial}{\partial x}\left(\mu_{eff}\frac{\partial u}{\partial z}\right)+\frac{\partial}{\partial y}\left(\mu_{eff}\frac{\partial v}{\partial z}\right)+\frac{\partial}{\partial z}\left[\mu_{eff}\frac{\partial w}{\partial z}-\frac{2}{3}(\rho k+\mu_{eff}\nabla\cdot\vec{u})\right]+g(\rho_\infty-\rho)$
e	$\frac{\mu_{eff}}{\sigma_e}$	$-p\nabla\cdot\vec{u}-\nabla\dot{q}_{rad}$
k	$\frac{\mu_{eff}}{\sigma_k}$	$G_k+G_B-\rho\varepsilon$
ε	$\frac{\mu_{eff}}{\sigma_\varepsilon}$	$\frac{\varepsilon}{k}[C_1(G_k+C_4G_B)-C_2\rho\varepsilon]+C_3\rho\varepsilon\nabla\cdot\vec{u}$
f	$\frac{\mu_{eff}}{\sigma_f}$	0

$G_k=\mu_{eff}\left(\frac{\partial u_i}{\partial x_j}+\frac{\partial u_j}{\partial x_i}\right)\frac{\partial u_i}{\partial x_j}$, $G_B=\frac{\mu_{eff}}{\sigma_t}g\frac{1}{\rho}\frac{\partial\rho}{\partial z}$, $\mu_{eff}=\mu+\mu_t$

σ_k=1.0, σ_ε=1.22, σ_e=0.64, σ_f=1.0, σ_t=0.7, C_μ=0.09, C_1=1.44, C_2=1.92, C_3=−0.343, C_4=1.44 for $G_B>0$ and is zero otherwise.

for mass, momentum, gas species concentration and internal energy. Turbulence is modeled using the modified $k-\varepsilon$ equation model which were included to allow for the production of turbulence due to buoyancy and the effect of thermal stratification of the turbulence dissipation rate. We consider a thermally expandable ideal gas driven by a prescribed heat source. The equations of motion governing the fluid flow are written in a form suitable for low Mach number applications. Sometimes, this form of the equations is referred to as weakly compressible. The most important feature of these equations is that in the energy equation the spatially and temporally varying pressure is replaced by an average pressure which depends only on time. The eight conservation equations were cast into the following form:

$$\frac{\partial}{\partial t}(\rho\phi)+\frac{\partial}{\partial x_j}(\rho u_j\phi)=\frac{\partial}{\partial x_j}\left(\Gamma_\phi\frac{\partial\phi}{\partial x_j}\right)+S_\phi \quad (1)$$

The variables, together with the exchange coefficients and source terms, are given in Table 1.

Equation (1) can be discretized as the following form.[18]

$$a_P\phi_P=\sum a_{nb}\phi_{nb}+b \quad (2)$$

where,

$$a_P=\sum a_{nb}+\rho\frac{\triangle V}{\triangle t}+S_P$$
$$b=S_C+\rho_P^0\phi_P^0\frac{\triangle V}{\triangle t} \quad (3)$$

Where the subscripts nb denotes a neighbor node, and the summation is to be taken over all the neighbors. Finite volume method and PISO algorithm are then employed for solving the linked set for velocity and pressure equations. The mathematical derivation and the experimental verification of the results are reported elsewhere[19,20] and will not be repeated here.

3.2 Combustion model

In the present numerical analysis, combustion products are discharged vertically upwards from pool source placed in the floor. Gas present in the room becomes a mixture of air (O_2 and N_2), fuel and combustion products (H_2O and CO_2). The combustion model is based on the global single-step irreversible form

$$1\text{ kg fuel}+s\text{ kg air}\rightarrow(1+s)\text{ kg products} \quad (4)$$

where s is the stoichiometric oxidant requirement of the fuel. To express the turbulent chemical source term in the species equation, it is often convenient to rewrite the equations in a form which does not contain any source term by introducing the mixture fraction f as a dependant variable. It is useful to describe the mixture field and to identify the location of the stochiometric mixture. The mixture fraction is defined from

$$f=\frac{\Phi-\Phi_\infty}{\Phi_F-\Phi_\infty},\quad\text{with}\quad\Phi=Y_{fu}-\frac{Y_{ox}}{s} \quad (5)$$

where Y_{fu}, Y_{ox} are the respective mass fractions of fuel and oxidant and the subscripts F, ∞ refer to fuel and oxidant streams for Φ, respectively.

The species conservation equations may then be written as

$$\frac{\partial}{\partial t}(\rho\bar{f})+\frac{\partial}{\partial x_j}(\rho u_j\bar{f})=\frac{\partial}{\partial x_j}\left(\frac{\mu_{eff}}{\sigma_f}\frac{\partial\bar{f}}{\partial x_j}\right)+S_f \quad (6)$$

where σ_f is the Prandtl/Schmidt number for $f(\sigma_f=0.7)$ and S_f is due solely to phase change. $S_f=0$, if there is no phase change.

The composition of the mixture is deduced from the determination of f by using the following relation

air excess :

$$0 \le f \le f_{sto} \Rightarrow Y_{ox} = Y_{ox,\infty}\frac{f_{sto}-f}{f_{sto}},\quad Y_{fu}=0$$

fuel excess :

$$f_{sto} \le f \le 1 \Rightarrow Y_{fu} = \frac{f-f_{sto}}{1-f_{sto}},\qquad Y_{ox}=0 \quad (7)$$

$$Y_{N2} = Y_{N2,\infty}(1-f)$$

$$Y_{pr} = 1 - Y_{fu} - Y_{ox} - Y_{N2}$$

where the stoichiometric value of f is $f_{sto} = [Y_{ox,\infty}/s]/[1+Y_{ox,\infty}/s]$.

3.3 Radiation model

Radiant energy lost by the plume increases significantly temperature of the surrounding surfaces and modifies temperature and heat exchanges in the room. Radiation is produced by hot heteronuclear gas molecules and by soot particles. Soot production mechanisms are difficult to describe and depend on fuel nature and combustion conditions. We don't take account for their effects in the radiation model.

The radiative transfer equation describing the intensity, I, in a rectangular absorbing, emitting and anistoropically scattering medium is

$$\left[\mu\frac{\partial}{\partial x}+\eta\frac{\partial}{\partial y}+\xi\frac{\partial}{\partial z}+\beta(x,y,z)\right]I(x,y,z,\Omega) = S(x,y,z,\Omega) \quad (8)$$

where

$$S(x,y,z,\Omega) = a(x,y,z)I_b(x,y,z) + \frac{\sigma_s(x,y,z)}{4\pi}\int_{\Omega'} I(x,y,z,\Omega')\Phi(\Omega';\Omega)d\Omega'$$

β=extinction coefficient

$\Omega(\mu,\xi,\eta)$=ordinate direction

a=absorption coefficient

σ_s=scattering coefficient

ϕ=phase function

subscript b=black body

superscript $'$=(prime) incoming value

The S-N discrete ordinates method replaces the radiative transfer equation with a set of equations for a finite number of M ordinate directions.[21] For a specific ordinate direction m, defined by $\Omega_m(\mu_m,\xi_m,\eta_m)$, the integral in the source term (equation (8)) is replaced by a Gaussian quadrature of order M with the appropriate angular weights w_m

$$S_m(x,y,z,\Omega) = a(x,y,z)I_b(x,y,z) + \frac{\sigma_s(x,y,z)}{4\pi} \times \sum_{m'=1}^{M} w_{m'}I_{m'}(x,y,z,\Omega_{m'})\Phi(\Omega_{m'};\Omega_m) \quad (9)$$

Also the average incident radiation G and the radiative heat fluxes Q_r are obtained as

$$G(x,y,z) = \frac{1}{4\pi}\sum_{m=1}^{M} w_m I_m(x,y,z) \quad (10)$$

$$Q_{rx}(x,y,z) = \sum_{m=1}^{M}\mu_m w_m I_m(x,y,z) \quad (11)$$

$$Q_{ry}(x,y,z) = \sum_{m=1}^{M}\xi_m w_m I_m(x,y,z) \quad (12)$$

$$Q_{rz}(x,y,z) = \sum_{m=1}^{M}\eta_m w_m I_m(x,y,z) \quad (13)$$

To solve the discrete ordinates equation, the rectangular room is subdivided into small control volumes. Within each control volumes, the spatially discretized equation for the radiative intensity in the ordinate direction Ω_m is derived as[13]

$$\mu_m(A_E I_{E,m} - A_W I_{W,m}) + \eta_m(A_N I_{N,m} - A_S I_{S,m}) + \xi_m(A_U I_{U,m} - A_D I_{D,m}) + \beta_P I_{P,m}\triangle V = a_P I_{bP}\triangle V + \frac{\sigma_{sP}}{4\pi}\triangle V \sum_{m'=1}^{M} w_{m'}\Phi_{m'm}I_{P,m'} \quad (14)$$

where E, W, N, S, U and D are the boundaries

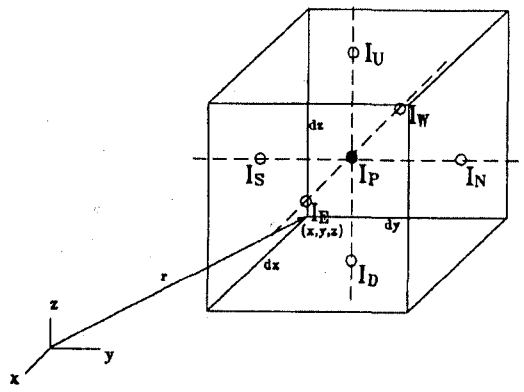

Fig. 2 Location of the average intensities and the differential CV in the x-y-z coordinate system.

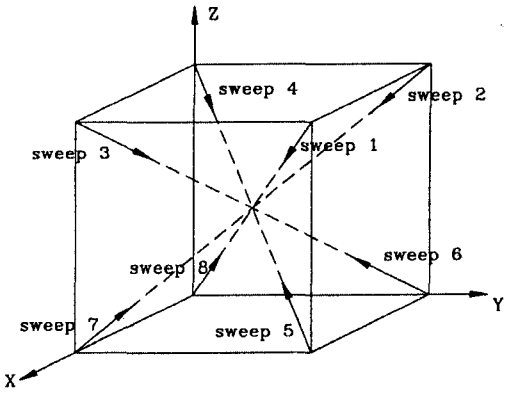

Fig. 3 Schematic diagram of the 8 sweep directions.

in the compass directions and P is the center point of the control volume. The area and volume elements are $A_E = A_W = \triangle y \triangle z$, $A_N = A_S = \triangle x \triangle z$, $A_U = A_D = \triangle x \triangle y$ and $\triangle V = \triangle x \triangle y \triangle z$, respectively. Figure 2 shows the location of the average radiative intensities. The solution of equation (14) approximates the solution of the radiative transfer equation (8). To calculate the discretized equation (14) in three-dimensional space, the 8 sweep directions are considered according to a sign of μ_m, η_m and ξ_m as shown Figure 3. The number of unknown I's in equation (14) is reduced by using one of several relationships between the control volume boundary intensities and the center point intensity. The weighted diamond difference scheme is used in this study to relate the intensities in the control volume.[22,23]

The total emissivity is equal to the absorption coefficient for a gray gas[24] and evaluated from the weighted sum of gray gases model (WSGGM) proposed by Schmidt et al.[25]

$$\varepsilon = \sum_{i=0}^{I} a_{\varepsilon,i}(T)[1 - \exp(-\kappa_i ps)] \qquad (15)$$

where $a_{\varepsilon,i}$ which depend on the gas temperature T denote the emissivity weighting factors for the i-th gray gas. The bracketed quantity is the i-th gray gas emissivity with absorption coefficient, κ_i, and pressure-path length product, ps. For a gas mixture ps is the sum of the partial pressures of the absorbing gases. In the present analysis, three component gray gases are considered to represent the emissivity of the mixture (carbon dioxide, water vapor, and air). The expressions for the coefficients of the WSGGM are taken from the work of Schmidt et al.[25]

4. Numerical method

In SMEP field model,[26] the difference schemes for discretizing the time term and the convection term into linear form used the Euler implicit scheme and the hybrid scheme respectively. The computations were carried out on a Pentium III 600 personal computer. In order to correctly model the smoke movement in the doorway, the numerical grid was extended by 50 percent in length (x direction) to include a region outside the fire compartment. A mesh of 13044 cells (11178 internal and 1866 external cells) in total was used to discretize the geometry for comparison with the room fire ex-

periment.[17] For experiments using methanol as a fuel, the three rooms used 10634 cells (9200 internal and 1434 external cells) for fire strength 7.65 kW, 9014 cells (7728 internal and 1286 external cells) for fire strength 21.25 kW and 13278 cells (11600 internal and 1678 external cells) for fire strength 51.71 kW, respectively. The mesh was non-uniformly distributed with refinements in the wall, floor, ceiling, fire and doorway regions. Within each time step, convergence was assumed if either the maximum number of iterations (100) was reached or the mass source residual fell to 1×10^{-3}. The time step used was 0.025 s and experiment and simulation was performed up to ten minutes as this was considered sufficient time for smoke movement to arrive at the steady state. With regard to computing time, the SMEP was executed on a Pentium III 800 PC and the computing time required was less than seven hours.

4.1 Boundary and initial condition

The initial temperature and pressure were set to be 293 K(300 K for Stecker's room fire experiment) and 101,325 Pa. The insulating walls of the room were modeled with no-slip conditions for the velocities and adiabatic conditions for the temperature. A fixed pressure boundary condition was used on all external boundaries. In the present calculation, the wall functions are used to bridge the near wall region as follows.

$$\tau_w = \frac{\rho C_\mu^{1/4} k_p^{1/2} \varkappa U_p}{\ln(E y_p^+)} \tag{16}$$

where

$$y_p^+ = \frac{\rho C_\mu^{1/4} k_p^{1/2} y_p}{\mu} \tag{17}$$

$\varkappa$=0.42 which is known as von Karmann constant. The subscript p refers to the first nodal point adjacent to the wall.

The wall boundary conditions to analysis the radiative heat transfer are all gray and diffusely reflecting, and they may also be sources for thermal radiation. The wall intensities are written as[23]

$$I_w(x,y,z,\Omega) = \varepsilon_w T_w^4(x,y,z) + \frac{1-\varepsilon_w}{\pi} \int_{\Omega'\cdot\vec{n}<0} |\Omega'\cdot\vec{n}|\, I_w(x,y,z,\Omega')d\Omega' \quad \text{for } \vec{n}\cdot\Omega>0 \tag{18}$$

Where $\vec{n}$ is the inward normal unit vector to the boundary wall and ε_w is the wall emissivity.

4.2 Plume model and inlet condition

The flame height depends on the fire geometry, the ambient conditions, the heat of combustion and the stoichiometric ratio. A relationship[27] for flame height that can be used for many fuels is

$$Z_{fl} = 3.3 Q_D^{*2/3} D_f \quad \text{for} \quad Q_D^* < 1 \tag{19}$$

$$Z_{fl} = 3.3 Q_D^{*2/5} D_f \quad \text{for} \quad Q_D^* > 1 \tag{20}$$

where,

$$Q_D^* = \frac{\dot{Q}}{\rho_\infty C_{p\infty} T_\infty (g D_f)^{1/2} D_f^2}$$

Where Z_{fl} is the mean flame height, in meters, $\dot{Q}$ is the heat release rate of the fire, in kW and D_f is the diameter of fire, in meters.

The virtual origin of the plume, $\triangle Z_f$(m),[28] is

$$\triangle Z_f = 1.02 D_f - 0.083 \dot{Q}^{2/5} \tag{21}$$

The virtual origin can be above the top of the

fuel or below the fuel. The sign convention is: for the virtual origin above the top of the fuel $\triangle Z_f$ is negative, and for the virtual origin below the top of the fuel $\triangle Z_f$ is positive. The mass flow, $\dot{m}$ (kg/s), of an axisymmetric plume at height Z_{fl}[29] is

$$\dot{m} = 0.071\dot{Q}_c^{1/3}(Z_{fl} + \triangle Z_f)^{5/3} \times [1 + 0.026\dot{Q}_c^{2/3}(Z_{fl} + \triangle Z_f)^{-5/3}] \quad (22)$$

where $\dot{Q}_c$ is the convective heat release rate of fire, in kW.

Smoke was defined to include the air that is entrained with the products of combustion. It follows that equation (22) can be thought of as an equation for the production of smoke from a fire. The average temperature of the plume can be obtained from a first law of thermodynamics analysis of the plume. For the steady plume the work is zero, and the changes in kinetic and potential energy are negligible. The first law leads to an equation for the plume temperature:

$$T_{zf} = T_\infty + \frac{\dot{Q}_c}{\dot{m}C_p} \quad (23)$$

where T_{zf} is the average plume temperature at elevation Z_{fl}, in K, T_∞ is the ambient temperature, in K and C_p is the specific heat of plume gases, in kJ/kgK.

Fire plumes consist primarily of air mixed with the products of combustion, and the specific heat of plume gases is generally taken to be the same as air. The density of air and plume gases is calculated from the perfect gas law. The absolute pressure is taken to be standard atmospheric pressure of 101,325 Pa, and the gas constant is taken to be that of air which is 287 J/kgK.

The vertical upward speed v at height Z_{fl} above a fire for thermal plumes in free spaces can be expressed as

$$v = \frac{\dot{m}}{A\rho_\infty} \quad (24)$$

where v is the vertical upward speed of plume at height Z_{fl}, in m/s, A is the fire source area and ρ_∞ is the density of ambient gas.

The inlet boundary conditions of fire source can be specified using the temperature T_{zf}, T_{cp} and velocity v obtained from the above equations.

5. Results and discussion

In the present study, results from a field model based on a self-developed SMEP code were compared with data obtained from the Steckler's room fire experiment. Figure 4 shows the temperature distribution of SMEP with and without radiation, FLOW3D without radiation, and experimental data[17] for doorway centerline temperature. A difference of more than 20℃ in the hot smoke layer is found between the temperature predicted by the SMEP and FLOW3D without radiation effect and obtained by the experimental result. On the other hand, the

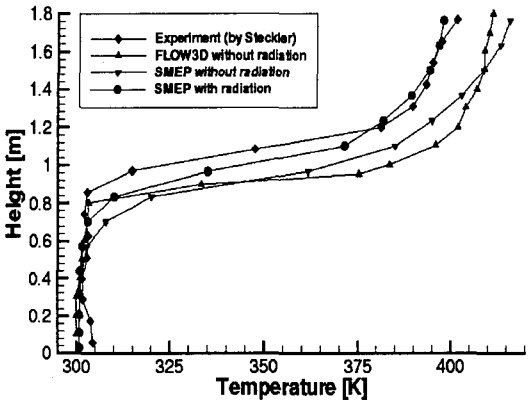

Fig. 4 Comparison of SMEP, FLOW3D and experimental data [17] for doorway centerline temperature.

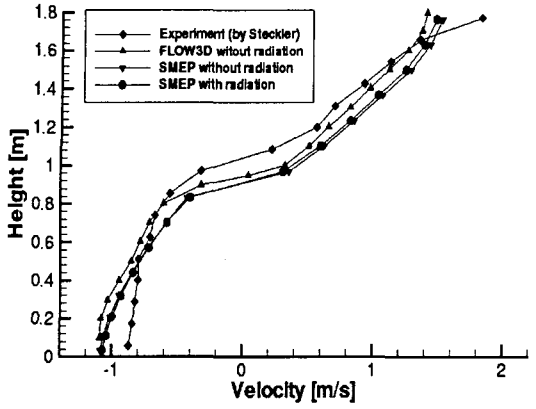

Fig. 5 Comparison of SMEP, FLOW3D and experimental data for doorway centerline velocity.

result of the SMEP with radiation effect has shown good agreement in comparison with the experimental data. These are thought to be due to the radiation effect of H_2O and CO_2 gas under smoke productions. Consequently, it shows that the radiation effect under smoke in fire should be specially considered in order to produce more realistic result.

The profiles of doorway centerline velocities are depicted in Figure 5 for the SMEP with and without radiation, the FLOW3D without radiation, and experiment.[17] The numerical results of the two codes produce good agreement in comparison with experimental data, however they tend to under-predict velocities in the upper most portion of the door. This result was also reported in the SMARTFIRE and PHOENICS predictions by Ewer.[5]

Figure 6(a) depicts temperature contour and velocity vector through the center of the room as predicted by SMEP with radiation using the 13044 cell mesh. As can be seen from the figure, the degree to which the fire plume is deflected backwards by the induced incoming flow. While it is extremely difficult to make accurate measurements, the inclination of the SMEP (Figure 6(a)) produced plume appears at approximately 50° to the horizontal. This result has shown about 7°~17° difference in comparison with the experimental observations—the (38±5)° to the horizontal—of Quintiere et al.[2] in an earlier series of experiments. Figure 6(b) depicts smoke concentration contour through the center of the room as predicted by SMEP with radiation. The smoke average concentration at the upper layer is about 15%. The smoke layer interface height (smoke concentration 5% point) in the doorway centerline appears to about 1m. This height shows the similar result in comparison with thermal interface height shown in

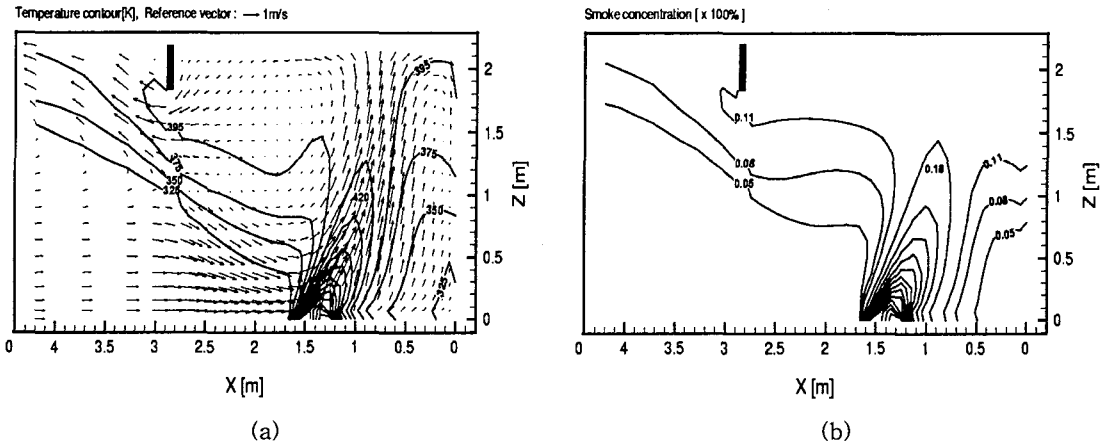

Fig. 6 Temperature distribution and velocity vector (a) and smoke concentration (b) through the center of the fire room passing through the doorway centerline produced by SMEP with radiation.

Table 2 Mass flow rates, neutral plane height and average upper layer temperature produced by SMEP with radiation, FLOW3D without radiation and experiment

Classification	Flux in [kg/s]	Flux out [kg/s]	Neutral plane height [m]	Average upper layer temp. [℃]
Steckler Experiment	0.554	0.571	1.027	129
SMEP with radiation	0.575	0.588	0.92	126
FLOW3D without radiation	0.582	0.591	0.926	134

Figure 6(a).

Table 2 shows the mass flow rates and neutral plane heights in the door and average upper layer temperature produced by SMEP, FLOW3D and experiment.[17] The SMEP results were produced from the simulation using the S-4 discrete ordinate method, in order to consider radiation influence. For the into and out mass flow rates through the opening, the SMEP with radiation produces the discrepancy of 4% and 3% respectively of the measured values, also the corresponding FLOW3D without radiation show the discrepancy of 5% and 4% respectively. The results reported in the JASMINE code (without radiation)[30] are within 8% and 11% respectively. For the neutral plane height, the two codes predict about within 11% in comparison with experimental result.[17] For the average upper layer temperature, the SMEP with radiation and FLOW3D without radiation predict results about within 3% and 4% of the measured values. The similar results were also reported in the PHOENICS predictions by Kerrison.[4] In conclusion, the results produced by SMEP using the S-N DOM radiation model showed good agreement with experiment and perform better than those produced using commercial CFD codes.

The temperature response at TC13 mounted on the top of door is illustrated in Figure 7. After the pool source using the methanol as a fuel was ignited, the steady time of the temperature distribution for fire sizes 7.65, 21.25 and 51.71 kW were approximately 390, 210 and 175 s respectively. As the fire size is increased from 7.65 kW to 51.71 kW, the steady time is observed to decrease and the amplitude of vibration is observed to increase as shown in Figure 7. The temperature response does fluctuate but not with a regular period. The gas temperatures in the present study are based on values measured after the steady time.

Figure 8 shows the comparison between the SMEP with radiation and experimental data con-

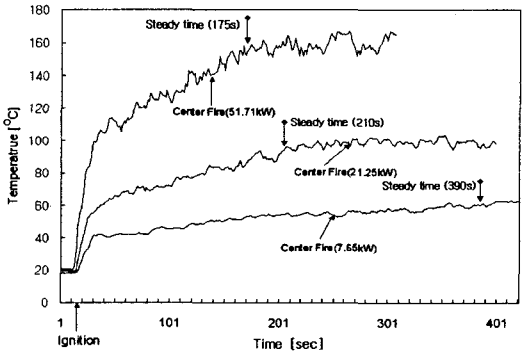

Fig. 7 Temperature distribution measured at TC13 by the fire size 7.65, 21.25 and 51.71 kW.

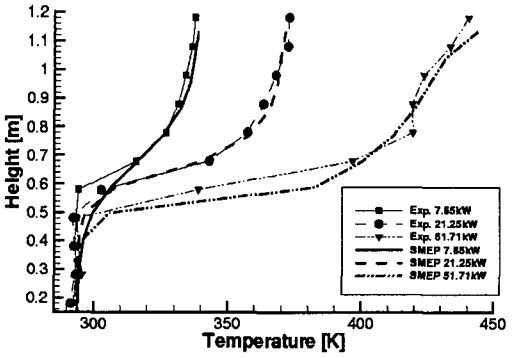

Fig. 8 Doorway centerline temperature of SMEP with radiation and experimental data for the fire size 7.65, 21.15 and 51.71 kW.

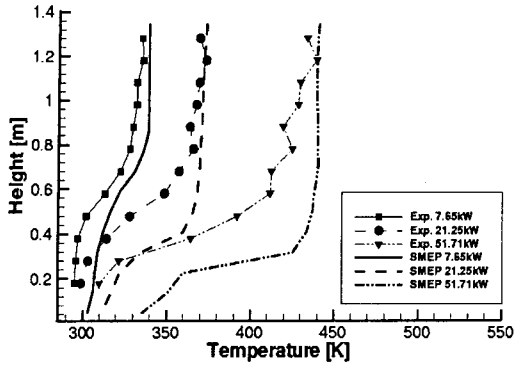

Fig. 9 Corner stack temperature of SMEP with radiation and experimental data for the fire size 7.65, 21.15 and 51.71 kW.

ducted by the authors for doorway centerline temperatures. The comparison between numerical result with radiation effect and experimental data has produced reasonable agreement. However SMEP with radiation for fire size 51.71 kW tend to over-predict temperature in the upper portion of the door. This seems to come from neglecting the heat transfer to ceiling wall by adiabatic condition.

Figure 9 depicts the corner stack temperatures for the SMEP with radiation and experimental data conducted by the authors. The SMEP with radiation provide a good approximation to the upper layer temperature. However, they tend to over-predict more than about 13% the lower layer temperatures. These are thought to be due to the problem of the wall boundary condition and turbulence model in the corner.

A summary of experimental and numerical results obtained by the authors is given in Table 3. The effective entrainment height in the door is determined from the thermal interface height deduced from the vertical temperature profile in the room. This height is determined by the position of rapid temperature change between the lower and upper portions of the room.[2] As the fire size is increased from 7.65 kW to 51.71 kW, the entrainment height in the doorway is observed to decrease. Throughout the simulations, SMEP with radiation has tended to underestimate the location of the neutral plane. This accuracy is thought to be due to the mesh resolution within the doorway. In computing $\dot{m}_a$ (air mass flow rate entrained through opening door [kg/s]) the mean upper and lower layer temperatures were selected from the temperature profile data as shown in Figure 8. The rate of air flow through the opening in the present experiment was estimated from the temperature data by the equation suggested by McCaffrey.[31] The $\dot{m}_a$ is obtained as

$$\dot{m}_a = 2.48 W_O \left[\frac{T_\infty}{T_u}\left(1-\frac{T_\infty}{T_u}\right)\right]^{1/2} (H_O - N)^{3/2} \quad (25)$$

where W_O is the width of the door in meters, H_O is the height of the door in meters and N is the height of the neutral plane in the door in meters. The neutral plane height was determined from the thermal interface height deduced from the vertical temperature profile in the room. As the fire size is increased from

Table 3 Summary of experimental and numerical results

Classification	Fire size Q [kW]	Entrainment height, N [m]	Flux in $\dot{m}_a$ [kg/s]	Flame / Fire plume angle [°]	Average hot layer temp. [℃]
Experiment	7.65	0.66	0.141	63±5	58
SMEP with Rad.	7.65	0.64	0.115	72	65
Experiment	21.25	0.64	0.191	55±5	94
SMEP with Rad.	21.25	0.63	0.152	69	97
Experiment	51.71	0.60	0.243	45±5	155
SMEP with Rad.	51.71	0.55	0.210	58	167

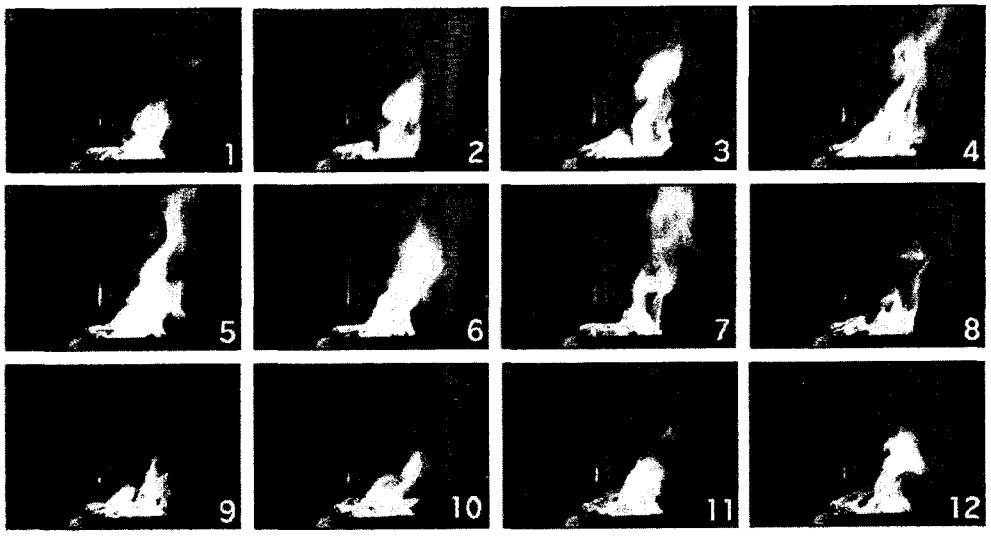

Fig. 10 Photographic series (Frames 1-12) of puffing flame, 0.25 m pool (21.25 kW fire) using methanol as a fuel.

7.65 kW to 51.71 kW, the air flow rate entrained through opening is observed to increase. Here the SMEP with radiation predicts the air mass flow rate to be within some 3% of the experimental results. This is to be expected as the air mass flow rate through the opening is entrained by the density difference deduced from the large temperature difference in the doorway. As the fire size is increased from 7.65 kW to 51.71 kW, the inclination of the flame deflected backwards by the induced incoming flow is observed to increase. This seems to come from the augmentation of the air entrainment rate through the opening according to the increase of the heat release rate. Also the inclination of the fire plume obtained from the SMEP result with radiation has shown a good agreement in comparison with the experimental observations. Photographs of Figure 10 are shown of a 21.25 kW flame stabilized on a 0.25 m pool. The photographs were taken with the digital video camera located at the side window (see Figure 1). The photographs of the visible flame were taken simultaneously with a time interval of 0.067 s. The flame angle for this case are shown the (55±5)° to the horizontal. In subsequent flames, the puffing pattern is repeated in a roughly periodic pattern with a mean period of about 0.67 s (from frame 1 to flame 11). Figure 11 shows the doorway centerline temperature distribution and velocity vector by SMEP with radiation for 21.25 kW fire. The inclination of the fire plume appears at approximately 69° to the horizontal. This has shown about 14° difference in comparison with the experimental observations (Figure 10). The average hot layer

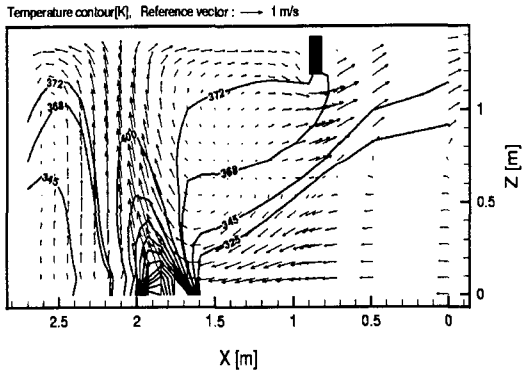

Fig. 11 Doorway centerline temperature distribution and velocity vector by SMEP with radiation for the fire size 21.25 kW.

temperature increases with increasing fire size. This temperature is determined by averaging the temperature values in the upper layer as measured by the thermocouple stack located in the corner of the room. The SMEP with radiation produces results average within 13% of the measured values.

6. Conclusions

To validate a self-developed SMEP field model, the SMEP results were compared with the Steckler's room fire experiment and commercial CFD package (FLOW3D). For the SMEP using S-N discrete ordinate model the predictions of the temperature, velocity, air mass flow rate and neutral plane height in the doorway centerline have shown good agreement in comparison with experiment and FLOW3D result. In particular the SMEP with radiation perform better than those produced using without radiation. Also comparisons of SMEP with radiation and experiment undertaken from the authors for doorway centerline temperature, neutral plane height, air entrainment rate, flame angle and average hot layer temperature have shown reasonable agreement. Therefore the SMEP with radiation is recommended for three-dimensional radiation computations in the cases of fire in rectangular enclosures.

The numerical and experimental studies in room fires shows phenomena as follows. As the fire size is increased from 7.65 kW to 51.71 kW, the air flow rate entrained through opening, the inclination of the flame and the average hot layer temperature is observed to increase, on the other hand the entrainment height is observed to decrease.

An investigation of the smoke movement in room fires reveals that careful modeling such as radiation, turbulence and combustion model is essential in order to correctly predict measured trends. Furthermore, in order to confirm the developed code, it is necessary to practice the extremely accurate experiment. Further work in various fire model validation is currently underway.

References

1. Zukoski, E. E., Kubota, T. and Cetegen, B., 1981, Entrainment in fire plumes, Fire Safety J., Vol. 3, pp. 107-121.
2. Quintiere, J. G., Rinkinen, W. J. and Jones, W. W., 1981, The effect of room openings on fire plume entrainment, Combustion Science and Technology, Vol. 26, pp. 193-201.
3. Yang, K. T., 1994, Recent development in field modeling of compartment fires, JSME Int. J. Ser B, Vol. 37, No. 4, pp. 702-717.
4. Kerrison, L., Mawhinney, N., Galea, E. R., Hoffmann, N. and Pate, M. K., A comparison of two fire field models with experimental room fire data, Fire Safety Science-Proc. of the Fourth Int. Sym., pp. 161-172.
5. Ewer, J., Galea, E. R., Patel, M. K., Taylor, S., Knight, B. and Petridis, M., 1999, SMARTFIRE: An intelegent CFD based fire model, J. of Fire Prot. Engr., Vol. 10, No. 1, pp. 13-27.
6. Xue, H., Ho, J. C. and Cheng, Y. M., 2001, Comaprison of different combustion models in enclosure fire simulation, Fire Safety J., Vol. 36, pp. 37-54.
7. Spalding, D. B., 1971, Concentration fluctuation in a rount free jet, Chem. Eng. Sci., Vol. 26, p. 95.
8. Bilger, R. W., 1975, Turbulent jet diffusion flames, Progress in Energy and Combustion Sci., Vol. 1, p. 87.
9. Lockwood, F. C. and Shah, N. G., 1989, A new radiation solution method for incorporation in general combustion prediction procedures, Eighteenth Symposium (international) on Combustion, London, 1405.
10. Hoffmann, N. and Markatos, N. C., 1988, Thermal radiation effects on fire enclosures, Applied Mathematical Modeling, Vol. 12, p. 129.

11. Forney, G. P., 1994, Computing radiative heat transfer occurring in a zone fire model, Fire Sci. & Tech., Vol. 14, No. 1-2, pp. 31-47.
12. Keramida, E. P., Karayannis, A. N., Boudouvis, A. G. and Markatos, N. C., 1998, Radiative heat transfer in fire modeling, National Institute of Standards and Tech., NISTIR 6242.
13. Fiveland, W. A., 1984, Discrete-ordinates solutions of the radiative transport equation for rectangular enclosures, J. of Heat Transfer, Vol. 106, pp. 699-706.
14. Thynell, S. T. and Ozisik, M. N., 1987, Radiation transfer in isotropically scattering rectangular enclosures, J. Thermophys., Vol. 1, No. 1, pp. 69-76.
15. Menguc, M. P. and Viskanta, R., 1985, Radiative transfer in three-dimensional rectangular enclosures containing inhomogeneous, anistropically scattering media, J. Quant. Spectrosc. Radiat. Transfer, Vol. 33, No. 6, pp. 533-549.
16. Schmidt, T. F, Shen, Z. F. and Friedman, J. N., 1982, Evaluation of coefficients for the weighted sum of gray gas model, J. of Heat Transfer, Vol. 104, pp. 602-608.
17. Steckler, K. D, Quintiere, J. G. and Rinkinen, W. J., 1982, Flow induced by fire in a compartment, NBSIR 822520, National Bureau of Standards, Washington, DC.
18. Patankar, S. V., 1980, Numerical heat transfer and fluid flow, McGraw Hill-Washington, DC, pp. 25-40.
19. Peric, M., 1985, A finite volume method for the prediction of three dimensional fluid flow in complex ducts, Ph.D, Imperial College.
20. Issa, R. I., 1985, Solution of the implict discretised fluid flow equations by operator-spliting, Journal of Computational Physics, Vol. 62, No. 1, pp. 40-65.
21. Chandrasekhar, S., 1960, Radiative Transfer Dover, New York, pp. 149-150.
22. Kim, T. K. and Lee, H. O., 1988, Effect of anisotropic scattering on radiative heat transfer in two-dimensional rectangular enclosures, Int. J. Heat Mass Transfer, Vol. 31, No. 8, pp. 1711-1721.
23. Kim, T. K., 1990, Radiation and combined mode heat transfer analysis in absorbing, emitting and Mie-anisotropic scattering media using the S-N discrete ordinate method, Ph.D Thesis, University of Minnesota.
24. Modest, M. F., 1991, The weighted sum of gray gases model for arbitrary solution methods in radiative transfer, J. Heat Transfer, Vol. 113, pp. 650-656.
25. Smith, T. F., Shen, Z. F. and Friedman, J. N., 1982, Evaluation of coefficients for the weighted sum of gray gases model, J. of Heat Transfer, Vol. 104, pp. 602-608.
26. Jeong, J. Y., Ryou, H. S., Kim, S. C. and Kim, C. I., 2000, A numerical study of smoke movement in atrium fires with ceiling heat flux, Proc. of the Fourth Asia-Oceania Sym. on Fire Sci. and Tech., pp. 425-437.
27. Cox, G., 1995, Combustion fundamentals of fire, Academic Press, San Diego, CA., pp. 139-176.
28. Heskestad, G., 1983, Virtual Origins of Fire Plumes, Fire Safety J., Vol. 5, No. 2, pp. 109-114.
29. Heskestad, G., 1984, Engineering Relations for Fire Plumes, Fire Safety J., Vol. 7, No. 1, pp. 25-32.
30. Heskestad, G., 1986, Fire plume air entrainment according to two competing assumption, Twenty-first Sym. on Combustion, Comb. Ins, Pittsburgh, PA., pp. 111-120.
31. McCaffery, B. J., 1979, Purely buoyant diffusion flames: some experimental results, National Bureau of Standards. NBSIR 79-1910.